JOURNAL OF THE ELECTROCHEMICAL SOCIETY

SOLID-STATE SCIENCE
AND TECHNOLOGY

NOVEMBER
1989

Plasma-Enhanced Chemical Vapor Deposition of Silicon Dioxide Using Tetraethylorthosilicate (TEOS)

Ismail T. Emesh, Giulio D'Asti, Jacques S. Mercier,* and Pak Leung

Northern Telecom Electronics, Limited, Ottawa, Ontario, K1Y 4H7 Canada

ABSTRACT

This paper presents a study on plasma-assisted chemical vapor deposition of silicon dioxide films using tetraethylorthosilicate (TEOS). It was found that when oxygen is utilized as an oxidant, the resulting film contained approximately 1 atom percent (a/o) of nitrogen or carbon, whereas using N_2O in the reaction slightly increased the nitrogen concentration to 2 a/o. However, in the absence of oxidant, the carbon and nitrogen concentrations were approximately 18 and 6 a/o, respectively. The step coverage of the film, regardless of the oxidant, was approximately 34%, a substantial improvement compared to the 10% obtained for oxide films deposited using silane-based chemistry. The refractive index, infrared spectrum, and film density appear characteristic of deposited SiO_2 films. The electrical characterization of the TEOS-O_2 films yielded a breakdown electric field greater than 6.6 MV/cm, and a leakage current density of 8×10^{-9} A/cm^2 at 1 MV/cm. The breakdown electric field and leakage current density of a thermally grown oxide with comparable thickness are 8 MV/cm and 2×10^{-9} A/cm^2, respectively.

Silicon dioxide is used in the fabrication of MOS IC devices as a gate or an intermetal isolation dielectric, and as a passivation layer. Silane chemistry is commonly utilized to deposit intermetal dielectric films. However, this method produces films with unsatisfactory step coverage (1-2). The use of other silicon compounds, notably tetraethylorthosilicate (TEOS), has recently gained wide interest. TEOS can be thermally decomposed at a temperature higher than 600°C to give an oxide film with good step coverage. Unfortunately, the temperature required is too high for this process to be used over aluminum. Consequently, considerable efforts have been made in recent years to develop low-temperature, plasma-enhanced chemical vapor deposition (CVD) utilizing TEOS chemistry (3-4). In this study, the effect of the deposition parameters on the oxide film properties and deposition rate, using TEOS and O_2 as reactants, was first investigated. The film was then compared to films deposited with TEOS-N_2O and silane chemistries.

Experimental

Oxide films were deposited in a Reinberg-type plasma CVD batch reactor (22 wafers) (5), using an aluminum shower head electrode configuration modified to handle a TEOS source, which was contained in a stainless steel ampul. The TEOS was connected to the chamber by a 1.27 cm diameter stainless steel tube heated to 60°C to prevent condensation. A flow of nitrogen was maintained through the ampul to ensure liquid evaporation under the experimental conditions and to carry TEOS vapor into the reaction chamber.

In a typical deposition run, the 100 mm Si(100) wafers were heated under vacuum for 30 min to stabilize the thermal profile. Nitrogen and oxygen were then allowed to flow in at their process rates. During this time, TEOS was heated up to a preset temperature, after which nitrogen was allowed to flow through the ampul to introduce TEOS into the chamber. This predeposition cycle took approximately 3 min, after which the RF power was turned on for a predetermined time.

Unless otherwise stated, the deposition parameters were as follows:

1. substrate temperature = 260°C
2. total pressure = 360 mtorr
3. total flow rate = 1700 cm^3/min
4. O_2:N_2 (ampul):N_2 = 1.4:1.0:4.8
5. RF power = 225W (0.06W/cm^2)
6. TEOS temperature = 44°C.

The films were optically characterized by measuring the thickness and refractive index of the deposited films with a Tylan Tyger reflectometer using a He-Ne laser operating at $\lambda = 0.6328$ µm. The impurity levels in the films were determined by Auger. An Auger energy spectrum was taken from 30 to 2000 eV on each sample. Auger depth profiling was performed by sputtering with argon and measuring the oxygen KLL, silicon LMM, carbon KLL, and nitrogen KLL spectra. The sputter rate used for the profile was 106 Å/min and data was collected every 30s. The etch rates were measured at 25°C using P-etch (H_2O:HF:HNO_3 = 92.4:4.6:3.0 in volume) (6). The step coverage was measured using a SEM Cambridge Steroscan 250 at 20 kV. All samples were delineated in 50:1 buffered HF, then Au-Pd coated. The IR spectra were measured from 4000 to 400 cm^{-1} using a Nicolet 205X Fourier transform infrared (FTIR) spectrometer referred to an unprocessed silicon wafer of the same lot.

The electrical properties of the oxide film deposited on n-type (100) Si was investigated by measuring the breakdown voltage, leakage current, flatband voltage, and fixed charges using a MOS capacitor structure. The wafer surface was prepared by the growth and etch back of a 300Å layer of thermal oxide, after which films of approximately 500Å were deposited using TEOS-O_2-based chemistry. A thermally grown oxide film was also grown by the dry oxidation of Si in O_2 atmosphere at 1050°C and was used for comparison. The area of the upper n-type polysilicon electrode was about 0.008 cm^2. Current-voltage plots were obtained by increasing the voltage from 0 to 50V in 0.1V increments while the current was measured at each interval. High frequency (1 MHz) C-V plots were also ob-

---

*Electrochemical Society Active Member.

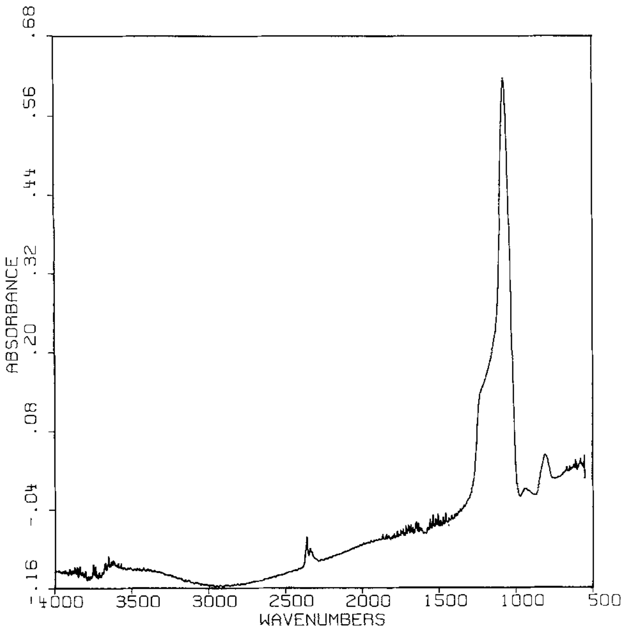

Fig. 1. Infrared spectrum of SiO_2 deposited at 330°C using TEOS-O_2

tained in order to calculate the flatband voltage (V_{FB}) and the oxide fixed change density Q_f/q.

Results and Discussion

General.—The refractive index of oxide films deposited at a temperature range of 260°-330°C with TEOS-O_2 chemistry was measured to be 1.47 ± 0.04. A deposition rate of 170 Å/min was obtained, with a film uniformity of ±2%, both across the wafer and from wafer to wafer. Deposition rates were found to be insensitive to change in the RF power (200-600W) under the present experimental conditions.

The infrared spectrum of the 5000Å-thick oxide film was measured with FTIR. Figure 1 shows an infrared spectrum of the oxide film which is characteristic of deposited SiO_2 film (7). The unannealed oxide film shows a weak band at 930 cm^{-1} and a broad band from 3200 and 3600 cm^{-1}. The latter probably resulted from adsorption of water vapor either from the plasma chamber or from the atmosphere. After annealing at 1050°C for 50s, there were no detectable amounts of impurities, as revealed by the disappearance of these bands in the IR spectrum.

The electric field breakdown for 500Å TEOS-O_2 films is greater than 6.6 MV/cm, as compared to 8 MV/cm for thermally-grown oxide film of similar thickness. The TEOS-O_2 film has a leakage current density of 8×10^{-9} A/cm^2, while the thermally-grown oxide exhibited a leakage current density of 2×10^{-9} A/cm^2 at 1 MV/cm. The TEOS-O_2 films deposited in this temperature range have V_{FB} near −0.6V and Q_f/q near 1×10^{11} cm^{-2}, which compares favorably to the thermal oxides with a V_{FB} of −0.3V and a Q_f/q close to 1×10^{10} cm^{-2} (8).

Auger analysis.—An Auger spectrum of an oxide film taken after removing the carbon residue from the surface by argon sputtering is shown in Fig. 2. The spectrum exhibits Auger features at 76, 503, and 1606 eV, which are characteristic of SiO_2, O, and Si, respectively. The Auger depth analysis of oxide film shown in Fig. 3, 4, and 5, are for oxide films deposited in oxygen, in N_2O, and in the absence of oxidant, respectively. In the presence of oxygen Fig. 3 shows that the nitrogen or carbon concentration is approximately 1 a/o. When N_2O is used as an oxidizing agent, Fig. 4 indicates that approximately 1 a/o of carbon and 2 a/o of nitrogen are incorporated into the oxide film, except at the SiO_2-Si interface, where an accumulation of impurities of 8-9 a/o is observed. This accumulation sug-

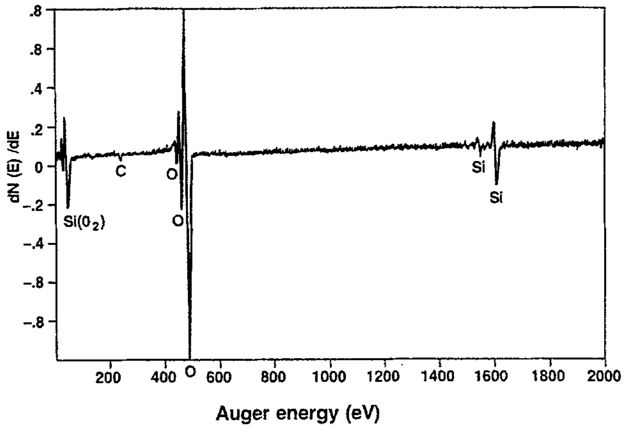

Fig. 2. Surface Auger spectrum of TEOS-O_2 film after removing carbon residue from the surface by Ar sputtering.

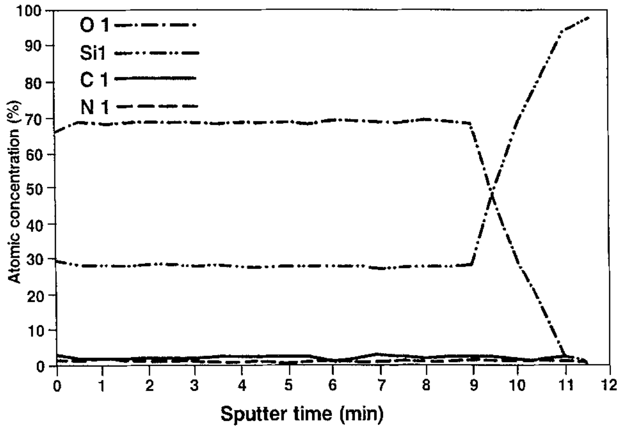

Fig. 3. Auger depth analysis of TEOS-O_2 film

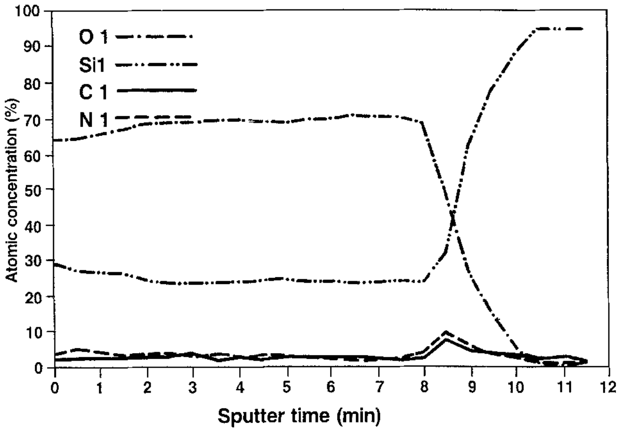

Fig. 4. Auger depth analysis of TEOS-N_2O film

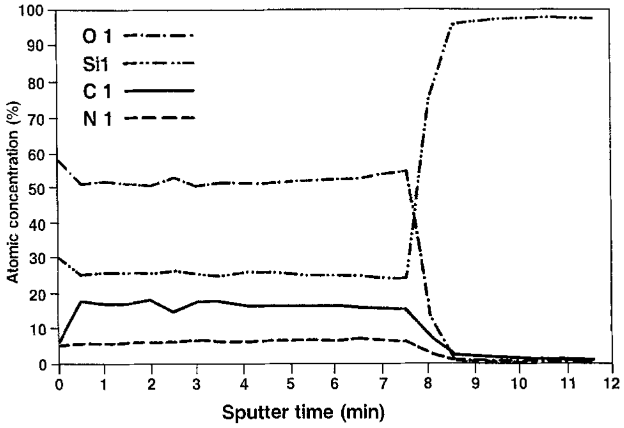

Fig. 5. Auger depth analysis of TEOS-N_2 film

Table I. Wet etch rates of various oxide films

Type of oxide	Deposition temperature °C	Etch rates (Å/s)
Thermally grown	950	2
Plasma TEOS-O_2	330	4
Plasma TEOS-N_2O	330	10
Plasma CVD SiH_4-N_2O	380	13
Thermal CVD SiH_4-O_2	410	13

gests that there is an incubation period before the N_2O starts participating in the deposition reaction.

In the absence of oxidant (Fig. 5), the film contains a high carbon concentration (18 a/o) and moderately high nitrogen concentration (6 a/o). It would appear that oxygen is required to scavenge away the carbon as volatile reaction products. The presence of carbon and nitrogen impurities may be accounted for by the higher refractive index of the oxide films, namely, 1.50 for TEOS-N_2O-SiO_2 films, compared to 1.47 for TEOS-O_2-SiO_2 films.

Wet etch rate.—The densification state of the oxide films was evaluated by wet etching using a P-etch solution. The wet etch rates of TEOS-O_2-SiO_2 and TEOS-N_2O-SiO_2 films, along with those of thermally grown SiO_2, and plasma-assisted and LPCVD SiO_2 films deposited with a SiH_4 chemistry, are given in Table I. With the exception of the thermally grown oxide film, the TEOS-O_2-SiO_2 film seems to be more densified than the other oxides.

The deposition temperature has a significant effect on the wet etching characteristics and therefore on the densification state of the oxide film. The etch rate of oxide films deposited at 195°C was 12 Å/s, compared to an etch rate of 4 Å/s for layers deposited at 330°C. After receiving an RTA cycle at 1050°C for 50s, the etch rates of both films were 3 Å/s. Since the impurity levels in both films were similar and there was no change in the film thickness, the decrease in the wet etch rate as a result of annealing is likely driven by the changes in the local bonding associated with densification (9).

Step coverage.—The increase in the packing density of highly integrated circuits requires the filling of small gaps between metal lines with CVD dielectric oxide, without leaving any voids. The presence of voids adversely affects the production yield and device reliability, as thinning of metal films occurs over sharp steps.

The SEM cross sections of Fig. 6 show the filling of spaces with aspect ratios of 0.35 (a, top) and 0.60 (b, bottom), with 1.7 μm-thick TEOS-O_2-SiO_2 film. A delineation etch in buffered HF of the cleaved samples, which is necessary to enhance interface contrast for scanning electron micrography (SEM), shows no voids in spaces with aspect ratios less than or equal to 0.6. The equivalent TEOS-N_2O-SiO_2 and silane-SiO_2 films are shown in Fig. 7 and 8, respectively, where voids near the lower corners of the steps have clearly been decorated, thereby revealing weaker regions in the oxide. The step coverage of the TEOS-based oxide films, defined as the ratio of the film thickness at the edge to that over the flat surface, is roughly 34%, compared to 10% for silane-based oxide film. The non-conformal coverage of silane-based chemistry films indicates that the

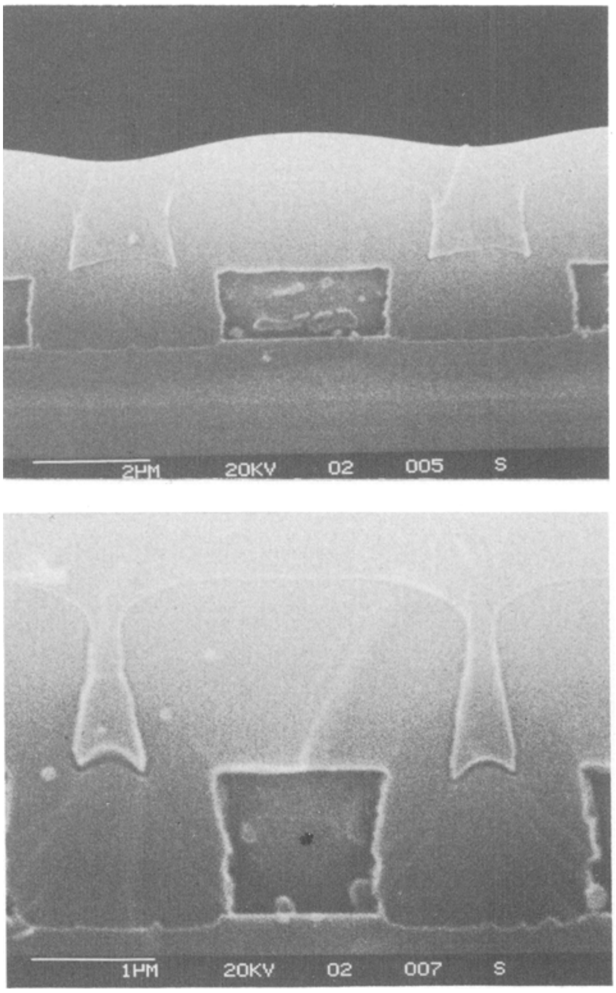

Fig. 6. SEM cross-sectional micrographs of TEOS-O_2-SiO_2 films after delineation etch in diluted HF. Aspect ratios are (a) 0.35, top, and (b) 0.60. Wafer was coated with photoresist. (Deposition conditions: F_{O_2} = 330 cm³/min, RF = 225W, T_{TEOS} = 55°C, $F_{N_2(bubbler)}$ = 370 cm³/min, F_{N_2} = 820 cm³/min, P = 450 mtorr, T_{Sub} = 260°C.)

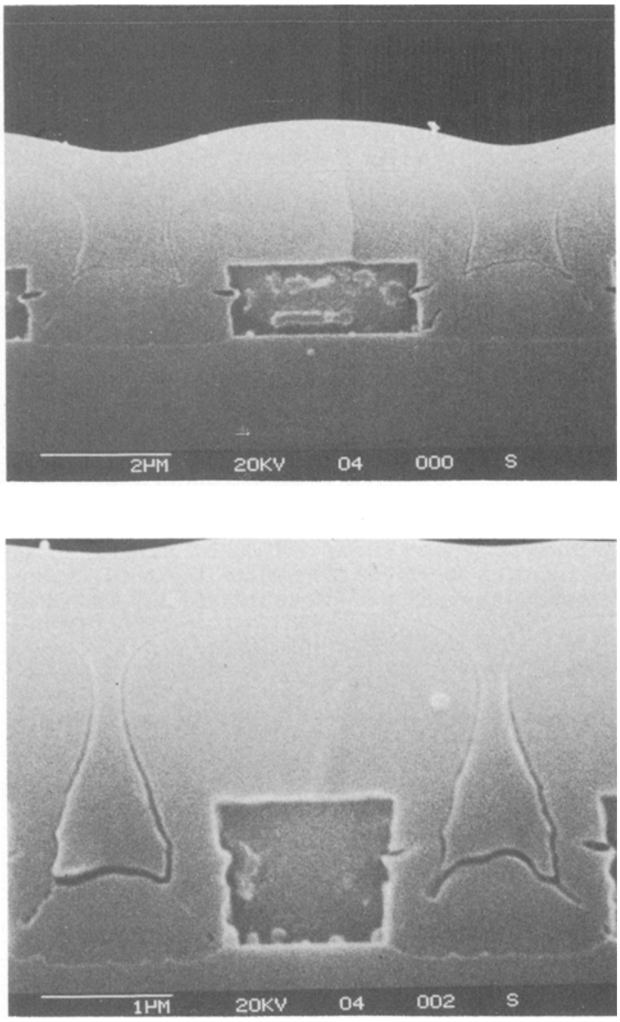

Fig. 7. SEM cross-sectional micrographs of TEOS-N_2O-SiO_2 films after delineation etch in diluted HF. Aspect ratios are (a) 0.35, top, and (b) 0.60. Wafer was coated with photoresist. (Deposition conditions: T_{TEOS} = 55°C, $F_{N_2(bubbler)}$ = 370 cm³/min, F_{N_2} = 800 cm³/min, F_{N_2O} = 1070 cm³/min, P = 450 mtorr, T_{sub} = 260°C, RF = 225W.)

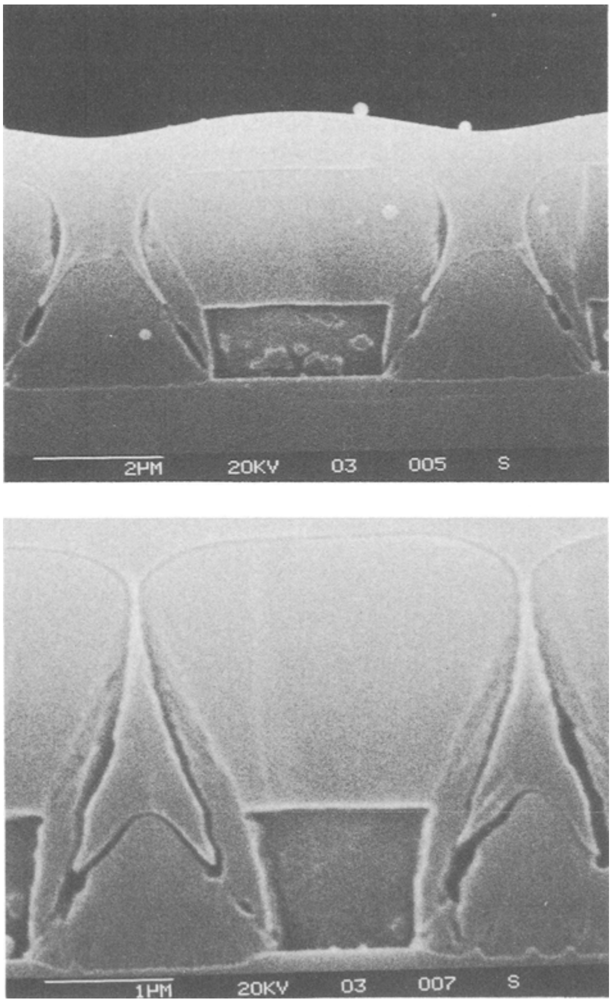

Fig. 8. SEM micrographs of SiH_4-O_2 SiO_2 films after delineation etch in diluted HF. Aspect ratios are (a) 0.35, top, and (b) 0.60. Wafer was coated with photoresist. (Deposition conditions: $F_{N_2} = 1060$ cm^3/min, $F_{SiH_4} = 500$ cm^3/min, $F_{N_2O} = 1560$ cm^3/min, $P = 354$ mtorr, $T_{sub} = 300$°C, RF = 250W.)

molecular mean free path for surface migration is probably less than 1 μm (10).

Although the step coverages of the oxide film produced by TEOS-O_2 or TEOS-N_2O are similar, there is more thinning of the film at the center of the gap with the N_2O than with the O_2. The oxide thickness at the center of the gap is approximately 85% for TEOS-O_2 as compared to 70% for that of TEOS-N_2O. In addition, the enhancement of the wet etch rate of the cleaved sample near the bottom step corners, mentioned above for TEOS-N_2O film, suggests that the surface migration of the adsorbed surface species is somewhat improved by replacing N_2O with O_2.

Deposition.—The effect of the deposition parameters of silane and TEOS process on uniformity, deposition rate, and refractive index was investigated using fractional factorial statistical design (11). The parameters, or factors, for the silane-based chemistry analysis included pressure, SiH_4/N_2O ratio, total flow rate, temperature and RF power. For the TEOS process, the parameters were pressure, TEOS temperature, carrier gas flow rate, RF power, and O_2 flow rate. The deposition parameters were varied by ±10% and the results obtained were analyzed statistically.

For deposition with silane chemistry, only the RF power had a significant effect. This is not surprising, as silane predominantly leads to the formation of active radicals such as NO, O, and SiH_3 in the plasma discharge (12-15). Therefore, increasing the RF power increases the concentration of these reactive species, which in turn increases the deposition rate. The substrate temperature was found to have little effect on the deposition rate in the range of 260°-330°C. Adams *et al.* (16) also reported a small dependency of the deposition rate on the temperature for such a range. Changing the deposition parameters had little effect on the uniformity of the oxide film. However, the refractive index was found to be proportional to the SiH_4/N_2O ratio, indicating that silicon-rich films were produced at the high end of the range studied (17).

Contrary to the silane-based chemistry, increasing the RF power from 200 to 600W had no effect on the deposition rate for the TEOS-O_2 process. However, in the absence of the plasma discharge, no deposition occurred in the temperature range used in this work. Therefore, it seems that an RF power as low as 200W (0.06 W/cm^2) is producing ion bombardment energies and fluxes sufficient to decompose TEOS molecules in the gas phase, and therefore is not the rate-limiting factor. The substrate temperature, the TEOS temperature, and the flow rate of the carrier gas had significant effects on the deposition rate of oxide films using TEOS, but had a lesser effect on the uniformity of the oxide film. None of the process variables had a significant effect on the film refractive index.

From the statistical analysis, the TEOS process is more sensitive to the changes in the deposition parameters than the silane-based process, particularly the TEOS temperature and the carrier gas flow rate. Therefore, for the TEOS to be used in a manufacturing process, where process stability is important, care must be taken to ensure that the liquid source temperature and the flow rate of the carrier gas remain constant. In addition, the feed line must be short and heated to prevent condensation.

The effect of oxygen partial pressure, TEOS partial pressure, and temperature on the deposition rate were also investigated. The dependence of the deposition rate on oxygen partial pressure was studied by varying the oxygen flow rates (0-300 cm^3/min). Figure 9 shows that the deposition rate increases with oxygen flows up to 75 cm^3/min, after which it saturates. Film deposition in this range is rate-limited by the amount of activated oxygen available to complete the oxidation of the active species. This view is supported by the reduction of carbon concentration in the film from 18 a/o in the absence of oxygen to approximately 1 a/o in the presence of oxygen (330 cm^3/min). A similar behavior was obtained when N_2O was used instead of O_2.

The dependency of the deposition rate on the TEOS vapor pressure was characterized by changing either the ampul temperature or the nitrogen flow rate through the ampul. At a constant liquid temperature, the increase in the nitrogen flow rate through the bubbler increased the deposition rate. Furthermore, the deposition rate increased with the increase in the liquid temperature while keeping the nitrogen flow rate constant. No attempt was made to measure the TEOS vapor pressure absolutely. We

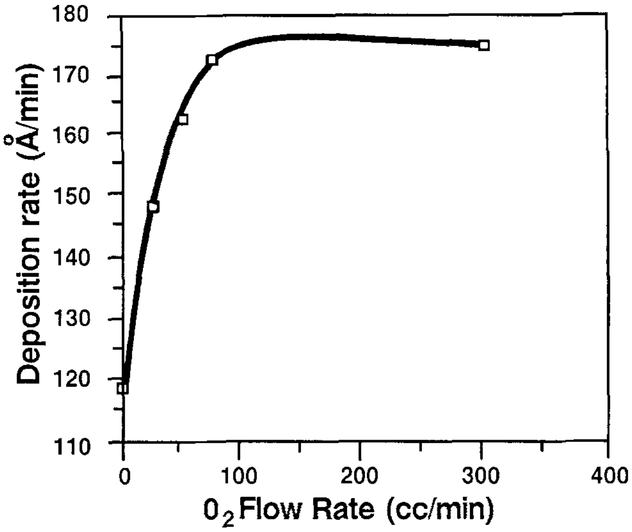

Fig. 9. Deposition rate of TEOS-O_2 films as a function of oxygen flow rate.

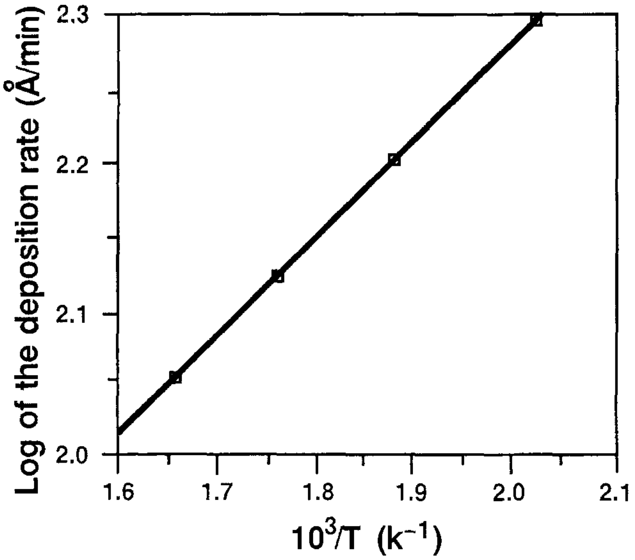

Fig. 10. Arrhenius plot of the deposition rate as a function of the substrate temperature.

assume that, at a fixed carrier flow rate and a constant pressure, the vapor pressure at a given temperature is proportional to the equilibrium vapor pressure. The logarithmic plot of the deposition rate *vs.* the partial pressure of TEOS gave a straight line whose slope is approximately 0.4. A zero-order, with respect to oxygen vapor pressure, was obtained. Thus, the rate expression for the deposition reaction may be written as

$$\text{rate} = K\, P_{\text{TEOS}}^{0.4} \times P^{o}_{O_2}$$

in agreement with the literature (18).

An Arrhenius plot for the deposition rates in the temperature range of 200°-330°C is shown in Fig. 10. The apparent activation energy of the deposition reaction is −3 kcal/mol. For thermally-driven reactions, raising the substrate temperature usually increases the deposition rate. However, the decrease in deposition rate observed here with increasing substrate temperature indicates that the oxide formation may be controlled by the adsorption of the reactive surface species. Increasing the substrate temperature enhances the desorption of the surface species, which in turn reduces the probability of the deposition reaction occurring. Another explanation of the negative activation energy is that the heat of adsorption of the reactive species is more negative than the (positive) activation energy of the deposition reaction. In any case, this interesting phenomenon needs to be further investigated to shed some light on the mechanism and to determine the active species involved in the deposition reaction.

Conclusion

Deposition of SiO_2 from TEOS and O_2 or N_2O in an RF plasma has been studied. The refractive index obtained for the films deposited with oxygen was 1.47, compared to 1.52 for TEOS-N_2O and TEOS only. Oxide films obtained by utilizing TEOS chemistry had 34% step coverage, as compared to 10% for films obtained through a silane-based chemistry. From Auger analysis, it was found that the use of oxygen as an oxidant minimizes the carbon and nitrogen impurities in the oxide film. The deposition process was found to be sensitive to the liquid TEOS temperature and the carrier flow rate. The deposition reaction order is approximately zero and 0.4 for O_2 and TEOS vapor pressure, respectively. An apparent activation energy of −3 kcal/mol was obtained, which suggests that the deposition is in an adsorption-controlled reaction regime. The electric field breakdown for the TEOS-O_2 oxide films was greater than 6.6 MV/cm, and a leakage current density of 8×10^{-9} A/cm^2 was observed.

Acknowledgments

We would like to thank Gerry Smith of BNR for the Auger analysis, Lisa Atkins for the SEM micrographs, and Paul McHugh for maintaining the deposition system in proper working condition.

Manuscript submitted Dec. 19, 1988; revised manuscript received April 13, 1989.

Northern Telecom Electronics, Limited, assisted in meeting the publication costs of this article.

REFERENCES

1. C. J. Santoro and D. L. Tolliver, *Proc. IEEE,* 59 (1971).
2. W. Kern, J. L. Vossen, and G. L. Schnable, 11th Ann. Proc. Reliab. Phys., p. 214, New York (1973).
3. L. J. Olmer, E. R. Lory, W. W. Clauhs, and A. Harrus, Abstract 255, p. 369, The Electrochemical Society Extended Abstracts, Vol. 87-1, Philadelphia, PA, May 10-15, 1987.
4. B. L. Chin and E. P. van de Ven, *Solid State Technol.,* **31,** (4), 119 (1988).
5. A. R. Reinberg, U.S. Pat. 3,757,733 (1973); *J. Electron. Mater.,* **8,** 345 (1979).
6. W. A. Pliskin and R. P. Gnath, *This Journal,* **111,** 872 (1964).
7. W. A. Pliskin, *J. Vac. Sci. Technol.,* **14,** 1064 (1977).
8. M. Simard-Normandin, I. Emesh, N. Pearce, G. D'Asti, and A. C. deWilton, *Can. J. Phys.,* **67,** 199 (1989).
9. P. G. Pai, S. S. Chao, Y. Takagi, and G. Lucovsky, *J. Vac. Sci. Technol.,* **A4,** 689 (1986).
10. R. M. Levin and K. Evans-Lutterodt, *J. Vac. Sci. Technol.,* **1,** 54 (1983).
11. G. E. P. Box, W. G. Hunter, and J. S. Hunter, "Statistics for Experimenters: An Introduction to Design, Data Analysis, and Model Building," John Wiley & Sons, New York (1978).
12. G. Lucovsky, P. D. Richards, D. V. Tsu, S. Y. Lin, and R. J. Markunas, *J. Vac. Sci. Technol.,* **A4,** 681 (1986).
13. P. D. Richard, D. V. Tsu, G. Lucovsky, and S. Y. Lin, *J. Non-Cryst. Solids,* **77-78,** 925 (1985).
14. P. D. Richard, R. J. Markunas, G. Lucovsky, G. G. Fountain, A. N. Mansour, and D. V. Tsu, *J. Vac. Sci. Technol.,* **A3,** 867 (1985).
15. P. A. Longeway, R. D. Estes, and H. A. Weakliem, *J. Phys. Chem.,* **88,** 73 (1984); P. A. Longeway, H. A. Weakliem, and P. D. Estes, *ibid.,* **88,** 3232 (1984).
16. A. C. Adams, F. B. Alexander, C. D. Capio, and T. E. Smith, *This Journal,* **128,** 1545 (1981).
17. S. M. Sze, "VLSI Technology," McGraw-Hill, New York (1983).
18. A. C. Adams and C. D. Capio, *This Journal,* **126,** 1042 (1979).